Relativistic positron beam generation by 10 PW laser

Yanjun Gu[1], Ondrej Klimo[1,2], Stefan Weber[1], and Georg Korn[1]

[1]Institute of Physics of ASCR, ELI-Beamlines, Na Slovance 2, Prague 18221, Czech Republic;
[2]FNSPE, Czech Technical University in Prague, 11519 Prague, Czech Republic;

ABSTRACT

In the laser-plasma interaction with ultra high intensity, the radiation reaction and gamma photon emission must be considered. The effects of quantum electrodynamics (QED) are significant when the emitted photon momentum becomes comparable to the momentum of the emitting electron. In this work, a regime of ultra-short relativistic positron beam generation by the ultra-high intensity laser-plasma interaction is proposed. A bunch of electrons are self-injected into the laser pulse due to the balance between electrostatic force and the laser ponderomotive force. These electrons can be confined in the laser pulse for a long time while emitting high energy gamma photons. The corresponding photons are counter-propagating through the strong laser field which provide a high probability for pair creation. Relativistic and well collimated positron beams are obtained.

Keywords: radiation reaction effect, pair-creation, laser-plasma interaction

1. INTRODUCTION

With the great development of the laser technology, the intensities up to 10^{22}W/cm^2 have been realized.[1] The forthcoming installations are expected to have the power of 10 PW with the peak intensities as high as 10^{23-24}W/cm^2.[2] In such a strong laser field, the radiation reaction and nonlinear Compton scattering in laser-plasma interaction should be considered. The γ-photons emitted in this case have large momentum which can be comparable to the emitting electrons and the interactions require the descriptions of QED. In this proceeding, we propose a regime of pair creation by using a 10 PW laser interacting with gas jet plasma.[3] The whole process can be divided in three stages. At first, a bunch of electrons are longitudinally injected into the laser pulse. By the interactions between the laser field and the electrons, a large number of γ-photons are emitted in the second stage, which provide a strong restoring force on the electrons and confine them inside the laser pulse. In the last stage, the counter-propagating photons collide with the laser field and generate the electron-positron pairs via the Breit-Wheeler process.[4,5]

2. METHODS

The PIC (Particle-in-Cell) simulations are performed with the relativistic electromagnetic code EPOCH.[6] A s-polarized Gaussian pulse is focused on the target boundary with the peak intensity of 10^{24} W/cm^2 and the corresponding normalized amplitude is $a_0 = eE_0/m_e\omega c \approx 850$, where E_0 and ω are the laser electric field strength and frequency, e and m_e are the electron charge and mass, respectively; and c is the speed of light in vacuum.

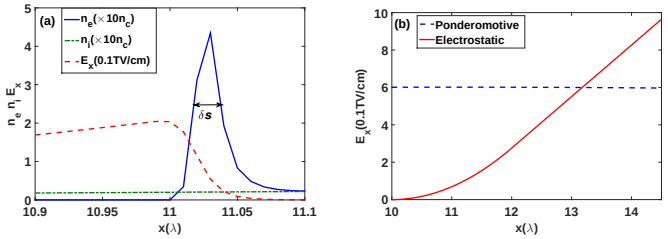

Figure 1. (a) The profiles of electron density (solid blue line), proton density (dash-dotted green line) and longitudinal electric field (dash red line) along the laser axis ($y = 0$) at $t = 37$ fs. (b) The evolution of the ponderomotive force field provided by the laser pulse at the foot of the pulse ($\eta = c\tau/\sqrt{2}$) on the laser axis ($r = 0$) and the electrostatic field estimated by the laser-piston model are plotted in dashed blue line and solid red line, respectively.

The laser pulse has a short duration with $\tau = 15$ fs and the beam waist is about $W_0 = 1.8\ \lambda$ (i.e. FWHM = 3 λ). A gas jet hydrogen plasma with the peak density of 4 n_c, where $n_c = m_e\omega^2/4\pi e^2$ is the plasma critical density, locates at $10\ \lambda < x < 34\ \lambda$ and $-15\ \lambda < y < 15\ \lambda$. The longitudinal density profile linearly increases to 4 n_c, then remains constant for $12\ \lambda < x < 32\ \lambda$, and then linearly decreases to 0. High resolution mesh size is used in the simulation as $\lambda/100$ and the corresponding timestep is $0.006\ \lambda/c$. About 120 million quasiparticles are employed. All simulations are performed with a realistic proton to electron mass ratio. Nonlinear Compton scattering and multiphoton Breit-Wheeler process are included in the simulations.

3. ELECTRON INJECTION INTO THE LASER FIELD

In this part, we discuss the mechanism of longitudinal electron self-injection. When the laser is propagating in the plasma, it expels the electrons away and generates a high density electron shell in front of the laser head like a piston. The profiles of the electron density, the ion density and the longitudinal electric field are presented in Fig. 1(a). The density peak formed at this moment reaches 45 $\mathrm{n_c}$. The high density electron shell provides a electrostatic field co-moving with the laser pulse. With the electron accumulation, the density of the shell becomes higher. According to a 1D piston model, we calculate the accumulated density as: $n_p = \int_0^l n_0 dl/\delta s = \int_0^t c n_0 dt/\delta s$, where $n_0 = 4n_c$ is the initial electron density and $l = ct$ is the propagation distance. The longitudinal electrostatic field given by the Possion's equation evolves with distance and time as: $\mathbf{E}_{static} = 2\pi n_p e \delta s$.

On the other hand, the effective field due to ponderomotive force can be derived as $\mathbf{E}_{pond} = \mathbf{F}_{pond}/e = -\nabla V_{pond}(x, y, z, t)/e$. With the increase of the accumulated electron peak, the ponderomotive force cannot sustain the pressure provided by the electrostatic field from the high density electron shell. Based on the above model, the trend of the electrostatic field and the laser ponderomotive field are plotted in Fig. 1(b). The electrostatic field is very close to the ponderomotive force field after the density peak propagates 12.8λ, which means a part of the electrons will be reflected by the electrostatic field and injected into the laser pulse. In this case, the electron density peak will accordingly decline due to the loss of the reflected electrons, which maintains the balance between the electrostatic field and the ponderomotive force field.

4. ELECTRON TRAPPING BY RADIATION DAMPING

When the longitudinal self-injection occurs, the electrons propagating through the pulse interact with the strong laser field. The dynamics and the trajectories of these electrons are significantly different in the case with and without considering the QED effects. The electrons cannot be confined inside the pulse in the NonQED case. However, if the QED effect is switched on, the injected electrons can stay in the pulse center for a long time and form a modulation structure, i.e. the injected electrons are trapped by the laser pulse. The displacement shift between the laser pulse and the QED electrons is very slow therefore the laser-electron interaction time is longer in the QED case compared to the NonQED case. The injection, trapping and modulation structures are displayed in Fig. 2(a) at 42 fs and (b) at 59 fs. The red, black and yellow dots represent the selected tracing electrons. Fig. 2(a) shows the electron accumulating stage and the electrons are pushed by the ponderomotive force in front of the laser head. It forms a typical plasma channel structure. The solid red line shows the longitudinal electric field corresponding to the left scale in the unit of TV/cm and the orange curve represents the laser intensity profile. To display the trapping electron layers clearly, the density is plotted in logarithmic as $\log_{10}(\mathrm{n_e}/\mathrm{n_c})$. Several electron layers are formed inside the channel from 14 λ to 16 λ in Fig. 2(b). The tracing electrons now locate in the different layers which means they have already been injected into the pulse center and have been trapped by the laser pulse. The distributions of the electron layers also show a modulation structure and the separation between each layer is half wavelength. It's due to the oscillating nature of the ponderomotive force, we see the electron bunches injected every half laser cycle.

Here we perform a couple of simulations of single electron interacting with the laser field. The initial conditions are read from one of the tracing particles in the previous simulation before the self-injection occurs. The electron start moving backwards with the longitudinal momentum $p_x = -700\ m_e c$. QED and NonQED cases are both considered and compared. The electron and photon longitudinal momentum evolution is plotted in Fig. 3(a). The net effect of the photon emission provides a negative momentum (dashed red line). It results that the backward drift of the electron is inhibited. This can be understood as a radiation damping force (restoring force)

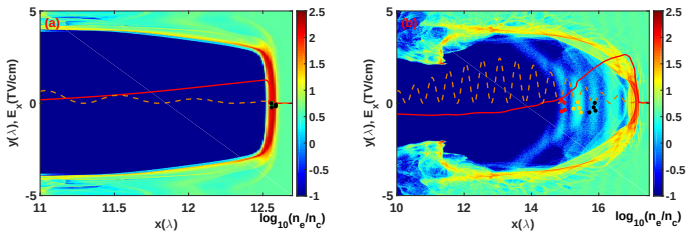

Figure 2. (a) and (b) are the electron density distribution (in log scale) at 42 fs and 59 fs. The colorful dots are the tracing particles located in different electron shells. The solid red line represents the longitudinal electric field.

in the Landau-Lifshitz form. The electron momentum (solid blue line) quickly becomes positive within 5 fs after emitting photons. The oscillation period of the electron momentum becomes larger, which can be regarded as the electron has to spend more time to penetrate through one laser period. The relative velocity between the laser pulse and the electron is much less than the initial state. In the NonQED case (dotted green line), the oscillation frequency is constant, which is much larger than the QED case. The electron cross the laser pulse at the speed of light. The electron slides down the poderomotive potential without picking up any longitudinal momentum which is consistent with the the laser vacuum acceleration regime. The longitudinal displacement of the single electron in different cases are plotted in Fig. 3(b) as a function of time. Before interacting with the laser field at about 35 fs, the motions of the electron in both cases are exactly the same. The QED electron is turned around after that while the propagation direction of the NonQED electron doesn't change. The displacement indicates the QED electron is co-propagating with the laser field. The velocity of the QED electron is slightly smaller than the speed of light (compare the slope of the blue solid line and the black dash-dotted line). Therefore, the trapped electron drifts slowly inside the laser pulse and will finally leave the laser field. Note that the negative photon momentum shown in Fig. 3(a) indicates the photons emitted by the longitudinal injection electrons are counter-propagating to the laser field. Furthermore, the photons are generated in the region of strong electromagnetic field, which makes the electron-positron pair creation become possible.

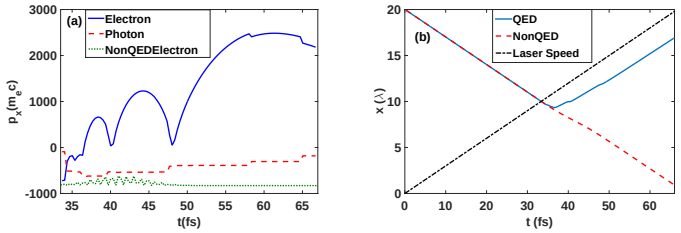

Figure 3. (a) is the longitudinal momentum evolution in the case of single particle dynamics simulations. The solid blue line indicates the electron momentum in the QED case. The dashed red line represents the sum of the total photons longitudinal momentum. The dashed green line is for the electron in NonQED case. (b) represents the longitudinal displacement of the electrons (blue solid for QED electron and red dashed line for NonQED) in the single particle dynamics simulations. The black dash-dotted indicates the laser field.

5. PHOTON AND POSITRON PRODUCTION

The trapped electrons are counter-propagating in the laser field and emit gamma-photons by nonlinear Compton scattering. In the single electron dynamics simulation, it's easy to follow the photons generated by a specified electron. Fig. 4(a) depicts the distribution of the parent electron and the generated photons. The curves represent the laser intensity contour lines. The electron is trapped in the strong field region and the photons are created on its path. The number of photons (super particle) is shown in Fig. 4(b) as time evolves. The threshold energy for the photons in the simulation is set to be 10MeV. The low energy photons are neglected. Within 10 T_0, the increase rate of photon creation is about 30 times. The decrease of the photon number after 67 fs is due to the escape of some photons on the boundary.

The electron-positron pair creation via Breit-Wheeler process[4,5] is induced by the gamma-photon colliding

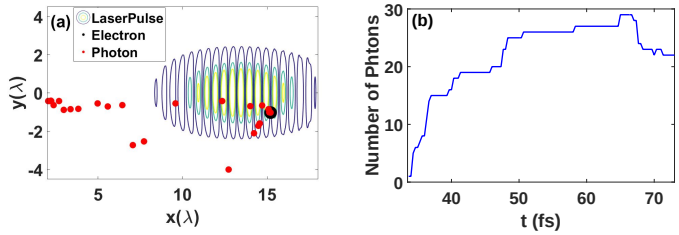

Figure 4. (a) The distribution of the electron (black dot), the generated photons (red dots) and the laser pulse intensity profile (curves) at 60 fs. (b) The photon number (super particle) with time evolution.

with the laser field. Fig. 5(a) depicts the positron density distribution at 100 fs. They follow the same modulated structure as the trapped electrons. The energy spectra of the positrons are plotted in Fig. 5(b). The peak energy is around 1 GeV. Furthermore, the positron bunch is highly collimated with a transverse emittance of 2.8 mm mrad. The positron bunches created in this regime can be used as an ideal external injection source for the further acceleration. The product rate of the positron in this case is about 3.11×10^6/J. Such nano-Coulomb positron bunches can be produced with the new generation of 10 PW laser facilities becoming available.[2]

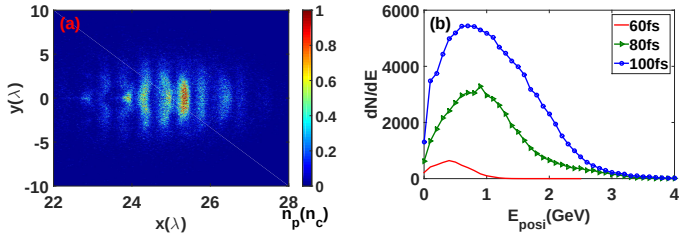

Figure 5. (a) The density distribution of positrons at 100 fs. (b) Temporal evolution of the positron energy spectra.

6. CONCLUSIONS

A mechanism for pair creation is proposed based on the interaction of 10 PW laser and gas jet plasma. The electron longitudinal self-injection is attributed for γ-photon emission and provide a large number of photons colliding with the laser field. The positron bunch with high energy and small transverse emittance is obtained. The results are beneficial for the potential experiments in the large laser facilities such as ELI project.[2]

ACKNOWLEDGMENTS

This work was supported by the project ELI: Extreme Light Infrastructure (CZ.02.1.01/0.0/0.0/15_008/0000162) from European Regional Development. Computational resources were provided by IT4Innovations Centre of Excellence under projects CZ.1.05/1.1.00/02.0070 and LM2011033 and by ECLIPSE cluster of ELI-Beamlines. The EPOCH code was developed as part of the UK EPSRC funded projects EP/G054940/1.

REFERENCES

1. V. Yanovsky, V. Chvykov, G. Kalinchenko, P. Rousseau, T. Planchon, T. Matsuoka, A. Maksimchuk, J. Nees, G. Cheriaux, G. Mourou, and K. Krushelnick, *Opt. Express* **16**, pp. 2109–2114, Feb 2008.
2. G. Mourou, G. Korn, W. Sandner, and J. Collier, *ELI Extreme Light Infrastructure (Whitebook)*, THOSS Media GmbH, 13187 Berlin, Germany, 2011.
3. Y. J. Gu, O. Klimo, S. Weber, and G. Korn, *New Journal of Physics* **18**(11), p. 113023, 2016.
4. G. Breit and J. A. Wheeler, *Phys. Rev.* **46**, pp. 1087–1091, Dec 1934.
5. A. I. Nikishov and V. I. Ritus, *Soviet Physics Uspekhi* **13**(2), p. 303, 1970.
6. C. Ridgers, J. Kirk, R. Duclous, T. Blackburn, C. Brady, K. Bennett, T. Arber, and A. Bell, *J. Comput. Phys.* **260**, pp. 273 – 285, 2014.